Conf-9411142--4

SAND94-2746C

MOVING MASS TRIM CONTROL FOR AEROSPACE VEHICLES

Rush D. Robinett
Beverly A. Rainwater
Shawn A. Kerr

Sandia National Laboratories
Albuquerque, NM

Abstract

A moving mass trim controller (MMTC) is proposed to increase the accuracy of axisymmetric, ballistic vehicles. The MMTC is different than other moving mass schemes because it generates an angle-of-attack (AOA) directly from the mass motion. The nonlinear equations of motion for a ballistic vehicle with one moving point mass are derived and provide the basis for a detailed simulation model. The full nonlinear equations are linearized to produce a set of linear, time-varying autopilot equations. These autopilot equations are analyzed and used to develop theoretical design tools for the creation of MMTCs for both fast and slow spinning vehicles. A fast spinning MMTC is designed for a generic artillery rocket that uses principal axis misalignment to generate trim AOA. A slow spinning MMTC is designed for a generic reentry vehicle that generates a trim AOA with a center of mass offset and aerodynamic drag. The performance of both MMTCs are evaluated with the detailed simulation.

Introduction

Over the years, techniques for controlling the flight characteristics of missiles and reentry vehicles (RV) have gravitated to systems that deliver relatively large amounts of control authority. For certain missions, such as an air-to-air missile or an RV designed to evade defenses, a large lateral acceleration capability was required. The technologies used to perform these missions ranged from actuated canards, elevons, and flaps to jet interaction, thrust vector control, and a variety of other techniques [1]. Because of inherent navigation inaccuracies, systems that provided modest amounts of control capability were of little or no value. However, with the maturity of the Global Positioning System (GPS), it is possible to mate simpler control techniques with GPS to increase the accuracy of existing systems. One such control technology is a moving mass controller. This technique has previously been evaluated in conjunction with other control methods such as the moving mass roll control of an aerodynamically asymmetric RV [2, 3]. A more direct application of moving mass control technology is the moving mass trim controller (MMTC). The MMTC generates a trim angle-of-attack (AOA) on an axisymmetric, ballistic vehicle directly from the motion of the mass. It is a novel, lightweight, low-cost retrofit to spinning ballistic vehicles that require modest flight path corrections to obtain increased accuracy.

Over ten years ago, initial studies of the MMTC were performed by Frank Regan at the Naval Systems Warfare Center (NSWC) [4]. Regan and his coworkers devised a single-shot MMTC that would provide modest range corrections near the target. At Sandia National Laboratories (SNL), the MMTC was an outgrowth of the Deconing Device Test (DDT) described by White and Robinett [5]. The DDT provided an initial glimpse of the effects of principal axis misalignment (PAM), roll rate, and center of mass offset. The MMTCs developed at SNL address the issue of roll rate, static margin (SM), PAM, and center of mass offset. The trim AOA for a fast spinning vehicle is generated by a PAM, whereas a slow spinning vehicle with a small static margin relies on a center of mass offset to create a trim AOA due to aerodynamic drag. This report derives the general nonlinear equations of motion for a one-moving mass system, the general linear, time-varying autopilot equations, and theoretical design tools, and develops conceptual hardware designs for a generic artillery rocket and a generic RV.

Equations of Motion

The system under consideration is shown in Figure 1. Rigid body B of mass m_B and moving point mass P of mass m_P combine to form system S of mass m_s, where $m_s = m_B + m_P$. Points of interest are B*, the mass center of B and S*, and the mass center of S. Coordinate frames are

This work was supported by the United States Department of Energy under Contract DE-AC04-94AL85000.

DISCLAIMER

DISCLAIMER

Portions of this document may be illegible in electronic image products. Images are produced from the best available original document.

the earth-centered inertial frame I, the local geodetic frame G comprised of north, east, and down unit vectors (denoted as $\bar{g}_1,\bar{g}_2,\bar{g}_3$), the body-fixed frame B (unit vectors $\bar{b}_1,\bar{b}_2,\bar{b}_3$), and the nonrolling frame N (unit vectors $\bar{n}_1,\bar{n}_2,\bar{n}_3$) which pitches and yaws but does not roll with B. Pitch, yaw, and roll are defined as a sequence of rotations as follows. After initial alignment of the G and B frames, rotations are performed in the following order: 1) yaw (angle ψ) about the $\bar{b}_3$ unit vector; 2) pitch (angle θ) about the new location of the $\bar{b}_2$ unit vector; and 3) roll (angle ϕ) about the final location of the $\bar{b}_1$ unit vector.

The mass may move in all three directions in the body, but its position, velocity, and acceleration in the B frame are controlled using third order actuator transfer functions in each direction. Therefore, the system is treated as having six degrees of freedom (6DOF).

Rolling Frame Equations of Motion

To verify results equations of motion expressed in the B frame were derived using two methods. Method 1 uses Newton's second law applied to S* to derive translational equations and equates the applied moments about S* to the derivative in the inertial frame of the inertial angular momentum of S for S* to derive rotational equations. Kane's method [6] is used in method 2.

Method 1:

The inertial angular velocity of B and the inertial velocity of B* are defined as

$$\overline{{}^{I}\omega}^{B} = \omega_1\bar{b}_1 + \omega_2\bar{b}_2 + \omega_3\bar{b}_3 \tag{1}$$

$$\overline{{}^{I}v}^{B^*} = v_1\bar{b}_1 + v_2\bar{b}_2 + v_3\bar{b}_3 \tag{2}$$

The mass ratio μ is defined as

$$\mu = \frac{m_p}{m_s} \tag{3}$$

The position vector from B* to P is given by

$$\bar{p} = p_1\bar{b}_1 + p_2\bar{b}_2 + p_3\bar{b}_3 \tag{4}$$

and the inertial velocity of S* is given by

$$\begin{aligned}\overline{{}^{I}v}^{S^*} &= [v_1 + \mu(\dot{p}_1 + \omega_2 p_3 - \omega_3 p_2)]\,\bar{b}_1 \\ &+ [v_2 + \mu(\dot{p}_2 + \omega_3 p_1 - \omega_1 p_3)]\,\bar{b}_2 \\ &+ [v_3 + \mu(\dot{p}_3 + \omega_1 p_2 - \omega_2 p_1)]\,\bar{b}_3\end{aligned} \tag{5}$$

The aerodynamic force is defined as

$$\bar{F}_{aero} = F_1\bar{b}_1 + F_2\bar{b}_2 + F_3\bar{b}_3 \tag{6}$$

and the force due to gravity is given by

$$\bar{F}_{grav} = m_s g\,({}^{G}X^{B}_{31}\bar{b}_1 + {}^{G}X^{B}_{32}\bar{b}_2 + {}^{G}X^{B}_{33}\bar{b}_3) \tag{7}$$

where g is the gravitational acceleration and ${}^{G}X^{B}$ is the direction cosine matrix relating the B frame to the G frame. The three elements of interest for the yaw, pitch, and roll sequence described previously are

$${}^{G}X^{B}_{31} = -\sin(\theta) \tag{8}$$

$${}^{G}X^{B}_{32} = \cos(\theta)\sin(\phi) \tag{9}$$

$${}^{G}X^{B}_{33} = \cos(\theta)\cos(\phi) \tag{10}$$

The torque about B* from aerodynamic forces is defined as

$$\bar{T}_{B^*} = T_1\bar{b}_1 + T_2\bar{b}_2 + T_3\bar{b}_3 \tag{11}$$

which results in a moment about S* of

$$\begin{aligned}\Sigma\bar{M}_{s^*} &= (T_1 - \mu p_2 F_3 + \mu p_3 F_2)\,\bar{b}_1 + \\ &(T_2 - \mu p_3 F_1 + \mu p_1 F_3)\,\bar{b}_2 + \\ &(T_3 - \mu p_1 F_2 + \mu p_2 F_1)\,\bar{b}_2\end{aligned} \tag{12}$$

The inertial angular momentum of S for S* is given by

$$\begin{aligned}\overline{{}^{I}H}^{s/s^*} &= \bar{I}^{B/B^*} \bullet \overline{{}^{I}\omega}^{B} \\ &+ \mu m_B\,(p_1\bar{b}_1 + p_2\bar{b}_2 + p_3\bar{b}_3) \times \overline{{}^{I}v}^{P} \\ &- \mu m_B\,(p_1\bar{b}_1 + p_2\bar{b}_2 + p_3\bar{b}_3) \times \overline{{}^{I}v}^{B^*}\end{aligned} \tag{13}$$

where the inertia dyadic of B for B* and for B frame unit vectors is defined as

$$\begin{aligned}\bar{I}^{B/B^*} &= B_{11}\bar{b}_1\bar{b}_1 + B_{12}(\bar{b}_1\bar{b}_2 + \bar{b}_2\bar{b}_1) \\ &+ B_{13}(\bar{b}_1\bar{b}_3 + \bar{b}_3\bar{b}_1) + B_{22}\bar{b}_2\bar{b}_2 \\ &+ B_{23}(\bar{b}_2\bar{b}_3 + \bar{b}_3\bar{b}_2) + B_{33}(\bar{b}_3\bar{b}_3)\end{aligned} \tag{14}$$

Evaluation of equation 13 yields

$$\begin{aligned}{}^{I}H^{s/s^*} &= \{B_{11}\omega_1 + B_{12}\omega_2 + B_{13}\omega_3 \\ &+ \mu m_B\,[p_2(\dot{p}_3 + \omega_1 p_2 - \omega_2 p_1) \\ &- p_3(\dot{p}_2 + \omega_3 p_1 - \omega_1 p_3)\,]\,\}\,\bar{b}_1\end{aligned}$$

$$+\{\ B_{12}\omega_1 + B_{22}\omega_2 + B_{23}\omega_3$$
$$+\mu m_B\,[p_3\,(\dot{p}_1 + \omega_2 p_3 - \omega_3 p_2)$$
$$-p_1\,(\dot{p}_3 + \omega_1 p_2\ \ -\omega_2 p_1\ ]\ \}\,\bar{b}_2$$
$$+\{B_{13}\omega_1 + B_{23}\omega_2 + B_{33}\omega_3$$
$$+\mu m_B\,[p_1\,(\dot{p}_2 + \omega_3 p_1 - \omega_1 p_3)$$
$$-p_2\,(\dot{p}_1 + \omega_2 p_3 - \omega_3 p_2)\ ]\ \}\,\bar{b}_3 \qquad (15)$$

From $\Sigma\bar{F}_{s^*} = m_s\,\bar{a}^{S^*}$ and

$$\frac{d}{dt}\,(\bar{H}^{s/s^*}) = \Sigma\bar{M}_{s^*}$$

the following six equations of motion may be obtained.

$$\dot{v}_1 + \mu p_3\dot{\omega}_2 - \mu p_2\dot{\omega}_3 = -\mu\ddot{p}_1 + 2\mu\omega_3\dot{p}_2$$
$$-2\mu\omega_2\dot{p}_3 - \omega_2\,[v_3 + \mu\,(\omega_1 p_2 - \omega_2 p_1)\ ]$$
$$+\omega_3\,[v_2 + \mu\,(\omega_3 p_1 - \omega_1 p_3)\ ] + g\,X^B_{31}$$
$$+F_1/m_s \qquad (16)$$

$$\dot{v}_2 - \mu p_3\dot{\omega}_1 + \mu p_1\dot{\omega}_3 = -\mu\ddot{p}_2 - 2\mu\omega_3\dot{p}_1$$
$$+2\mu\omega_1\dot{p}_3 - \omega_3\,[v_1 + \mu\,(\omega_2 p_3 - \omega_3 p_2)\ ]$$
$$+\omega_1\,[v_3 + \mu\,(\omega_1 p_2 - \omega_2 p_1)\ ] + g\,X^B_{32}$$
$$+F_2/m_s \qquad (17)$$

$$\dot{v}_3 + \mu p_2\dot{\omega}_1 - \mu p_1\dot{\omega}_2 = -\mu\ddot{p}_3 + 2\mu\omega_2\dot{p}_1$$
$$-2\mu\omega_1\dot{p}_2 - \omega_1\,[v_2 + \mu\,(\omega_3 p_1 - \omega_1 p_3)\ ]$$
$$+\omega_2\,[v_1 + \mu\,(\omega_2 p_3 - \omega_3 p_2)\ ] + g\,X^B_{33}$$
$$+F_3/m_s \qquad (18)$$

$$\left[B_{11} + \mu m_B\left(p_2^{\,2} + p_3^{\,2}\right)\right]\dot{\omega}_1$$
$$+\ (B_{12} - \mu m_B p_1 p_2)\,\dot{\omega}_2$$
$$+\ (B_{13} - \mu m_B p_1 p_3)\,\dot{\omega}_3 =$$
$$B_{23}\left(\omega_3^{\,2} - \omega_2^{\,2}\right) + \omega_1\,(B_{12}\omega_3 - B_{13}\omega_2) +$$
$$\omega_2\omega_3\,(B_{22} - B_{33}) - \mu m_B\,[2\omega_1\,(p_2\dot{p}_2 + p_3\dot{p}_3)$$
$$-2\dot{p}_1\,(p_2\omega_2 + p_3\omega_3) + p_2 p_3\left(\omega_3^{\,2} - \omega_2^{\,2}\right)$$
$$+\omega_2\omega_3\left(p_2^{\,2} - p_3^{\,2}\right) + p_1\omega_1\,(p_2\omega_3 - p_3\omega_2)$$
$$+p_2\ddot{p}_3 - p_3\ddot{p}_2\ ] + T_1 - \mu p_2 F_3 + \mu p_3 F_2 \qquad (19)$$

$$(B_{12} - \mu m_B p_1 p_2)\,\dot{\omega}_1$$
$$+\left[B_{22} + \mu m_B\left(p_1^{\,2} + p_3^{\,2}\right)\right]\dot{\omega}_2$$
$$+\ (B_{23} - \mu m_B p_2 p_3)\,\dot{\omega}_3 =$$
$$B_{13}\left(\omega_1^{\,2} - \omega_3^{\,2}\right) + \omega_2\,(B_{23}\omega_1 - B_{12}\omega_3) +$$
$$\omega_1\omega_3\,(B_{33} - B_{11}) - \mu m_B\,[2\omega_2\,(p_1\dot{p}_1 + p_3\dot{p}_3)$$
$$-2\dot{p}_2\,(p_3\omega_3 + p_1\omega_1) +$$
$$p_1 p_3\left(\omega_1^{\,2} - \omega_3^{\,2}\right) + \omega_3\omega_1\left(p_3^{\,2} - p_1^{\,2}\right) +$$
$$p_2\omega_2\,(p_3\omega_1 - p_1\omega_3) + p_3\ddot{p}_1 - p_1\ddot{p}_3\ ]$$
$$+T_2 - \mu p_3 F_1 + \mu p_1 F_3 \qquad (20)$$

$$(B_{13} - \mu m_B p_1 p_3)\,\dot{\omega}_1$$
$$+\ (B_{23} - \mu m_B p_2 p_3)\,\dot{\omega}_2$$
$$+\left[B_{33} + \mu m_B\left(p_1^{\,2} + p_2^{\,2}\right)\right]\dot{\omega}_3 =$$
$$B_{12}\left(\omega_2^{\,2} - \omega_1^{\,2}\right) + \omega_3\,(B_{13}\omega_2 - B_{23}\omega_1) +$$
$$\omega_1\omega_2\,(B_{11} - B_{22}) - \mu m_B\,[2\omega_3\,(p_1\dot{p}_1 + p_2\dot{p}_2)$$
$$-2\dot{p}_3\,(p_1\omega_1 + p_2\omega_2) + p_1 p_2\left(\omega_2^{\,2} - \omega_1^{\,2}\right) +$$
$$\omega_1\omega_2\left(p_1^{\,2} - p_2^{\,2}\right) + p_3\omega_3\,(p_1\omega_2 - p_2\omega_1) +$$
$$p_1\ddot{p}_2 - p_2\ddot{p}_1\ ] + T_3 - \mu p_1 F_2 + \mu p_2 F_1 \qquad (21)$$

Method 2:

Derivation of the rolling frame equations of motion using Kane's method follows.

The generalized inertia force equation is given by

$$F^*_r = -m_B {}^{I-B^*}v_r \bullet {}^{I-B^*}a - m_P {}^{I-P}v_r \bullet {}^{I-P}a + {}^{I}\bar{\omega}_r^{B} \bullet \bar{T}_B^{\,*} \qquad (r = 1,\ldots, 6) \qquad (22)$$

and the generalized active force equation is

$$F_r = {}^{I}\bar{\omega}_r^{B} \bullet \bar{T}_{B^*} + {}^{I-B^*}v_r \bullet \bar{F}_{B^*} + {}^{I-P}v_r \bullet \bar{F}_P \qquad (r = 1,\ldots, 6) \qquad (23)$$

In the following equations $u_i = \omega_i$ and $u_{i+3} = v_i$ (i = 1, 2, 3) from method 1.

The inertial angular velocity of B is

$${}^{I}\bar{\omega}^{B} = u_1\bar{b}_1 + u_2\bar{b}_2 + u_3\bar{b}_3 \qquad (24)$$

The inertial velocity of points B* and P are given below.

$${}^{I-B^*}v = u_4\bar{b}_1 + u_5\bar{b}_2 + u_6\bar{b}_3 \qquad (25)$$

$${}^{I-P}v = (\dot{p}_1 + u_4 + u_2p_3 - u_3p_2)\,\bar{b}_1 + (\dot{p}_2 + u_5 + u_3p_1 - u_1p_3)\,\bar{b}_2 + (\dot{p}_3 + u_6 + u_1p_2 - u_2p_1)\,\bar{b}_3 \qquad (26)$$

The generalized inertia torque for B is

$$\begin{aligned}\bar{T}_B^{\,*} = &-[B_{11}\dot{u}_1 + B_{12}\dot{u}_2 + B_{13}\dot{u}_3 + (B_{13}u_2 - B_{12}u_3)\,u_1 + B_{23}\left(u_2^{\,2} - u_3^{\,2}\right) + (B_{33} - B_{22})\,u_2u_3\,]\,\bar{b}_1\\ &-[B_{12}\dot{u}_1 + B_{22}\dot{u}_2 + B_{23}\dot{u}_3 + (B_{12}u_3 - B_{23}u_1)\,u_2 + B_{13}\left(u_3^{\,2} - u_1^{\,2}\right) + (B_{11} - B_{33})\,u_3u_1\,]\,\bar{b}_2\\ &-[B_{13}\dot{u}_1 + B_{23}\dot{u}_2 + B_{33}\dot{u}_3 + (B_{23}u_1 - B_{13}u_2)\,u_3 + B_{12}\left(u_1^{\,2} - u_2^{\,2}\right) + (B_{22} - B_{11})\,u_1u_2\,]\,\bar{b}_3\end{aligned} \qquad (27)$$

The aerodynamic force and its torque about B* are given by equations 6 and 11, respectively. The force due to gravity on point B* is

$$\bar{F}_{B^*_{grav}} = m_Bg\,({}^{G}X_{31}^{B}\bar{b}_1 + {}^{G}X_{32}^{B}\bar{b}_2 + {}^{G}X_{33}^{B}\bar{b}_3) \qquad (28)$$

The force on P is given by

$$\bar{F}_P = m_Pg\,({}^{G}X_{31}^{B}\bar{b}_1 + {}^{G}X_{32}^{B}\bar{b}_2 + {}^{G}X_{33}^{B}\bar{b}_1) \qquad (29)$$

No actuator force is applied to P or to a point of B due to the use of the actuator transfer function.

The partial velocities and partial angular velocities in equations 22 and 23 are found from equations 24 through 26. Using $F_r + F_r^* = 0$, solving the r=4 equation for $\dot{u}_4$, the r=5 equation for $\dot{u}_5$, and the r=6 equation for $\dot{u}_6$ in terms of $\dot{u}_1$, $\dot{u}_2$, and $\dot{u}_3$ yield equations of motion identical to those of method 1.

Nonrolling Frame Equations of Motion

It is desirable to write guidance algorithms using equations of motion for the nonrolling frame. Using the same approach as method 1 yields the following six equations of motion:

$$\begin{aligned}&m_s\dot{v}_{n1} + m_P\dot{p}_{n3}\dot{\omega}_{INn2} - m_P\dot{p}_{n2}\dot{\omega}_{INn3} =\\ &-m_P\ddot{p}_{n1} + 2m_P\omega_{INn3}\dot{p}_{n2} - 2m_P\omega_{INn2}\dot{p}_{n3}\\ &+m_s\,(\omega_{INn3}v_{n2} - \omega_{INn2}v_{n3})\\ &+m_Pp_{n1}\,(\omega^2_{INn2} + \omega^2_{INn3})\\ &-m_P\omega_{INn1}\,(p_{n2}\omega_{INn2} + p_{n3}\omega_{INn3})\\ &+m_B\dot{\phi}\,(\omega_{INn2}p_{n2} + \omega_{INn3}p_{n3})\\ &+m_sg\,{}^{G}X_{31}^{N} + F_{n1}\end{aligned} \qquad (30)$$

$$m_s\dot{v}_{n2}-m_P p_{n3}\dot{\omega}_{INn1}+m_P p_{n1}\dot{\omega}_{INn3}=$$
$$-m_P\ddot{p}_{n2}-2m_P\omega_{INn3}\dot{p}_{n1}+(2m_P\omega_{INn1}-m_B\dot{\phi})\dot{p}_{n3}$$
$$+m_s(\omega_{INn1}v_{n3}-\omega_{INn3}v_{n1})$$
$$+m_P p_{n2}(\omega^2_{INn1}+\omega^2_{INn3})$$
$$-m_P\omega_{INn2}(p_{n1}\omega_{INn1}+p_{n3}\omega_{INn3})$$
$$-m_B\dot{\phi}\omega_{INn1}p_{n2}-m_B\ddot{\phi}p_{n3}$$
$$+m_s g\,{}^G X^N_{32}+F_{n2} \qquad (31)$$

$$m_s\dot{v}_{n3}+m_P p_{n2}\dot{\omega}_{INn1}-m_P p_{n1}\dot{\omega}_{INn2}=$$
$$-m_P\ddot{p}_{n3}+2m_P\omega_{INn2}\dot{p}_{n1}$$
$$+(-2m_P\omega_{INn1}+m_B\dot{\phi})\dot{p}_{n2}$$
$$+m_s(\omega_{INn2}v_{n1}-\omega_{INn1}v_{n2})$$
$$+m_P p_{n3}(\omega^2_{INn1}+\omega^2_{INn2})$$
$$-m_P\omega_{INn3}(p_{n1}\omega_{INn1}+p_{n2}\omega_{INn2})$$
$$-m_B\dot{\phi}\omega_{INn1}p_{n3}+m_B\ddot{\phi}p_{n2}$$
$$+m_s g\,{}^G X^N_{33}+F_{n3} \qquad (32)$$

$$\left[N_{11}+\mu m_B\left(p^{\,2}_{n2}+p^{\,2}_{n3}\right)\right]\dot{\omega}_{INn1}$$
$$+(N_{12}-\mu m_B p_{n1}p_{n2})\dot{\omega}_{INn2}$$
$$+(N_{13}-\mu m_B p_{n1}p_{n3})\dot{\omega}_{INn3}=$$
$$-(N_{13}-\mu m_B p_{n1}p_{n3})\omega_{INn1}\omega_{INn2}$$
$$+(N_{12}-\mu m_B p_{n1}p_{n2})\omega_{INn1}\omega_{INn3}+$$
$$\left[N_{22}-N_{33}+\mu m_B\left(p^{\,2}_{n3}-p^{\,2}_{n2}\right)\right]\omega_{INn2}\omega_{INn3}$$
$$+(N_{23}-\mu m_B p_{n2}p_{n3})(\omega^2_{INn3}-\omega^2_{INn2})$$
$$-N_{11}\ddot{\phi}-2\mu m_B\omega_{INn1}(\dot{p}_{n2}p_{n2}+\dot{p}_{n3}p_{n3})$$
$$+2\mu m_B\dot{p}_{n1}(\omega_{INn2}p_{n2}+\omega_{INn3}p_{n3})$$
$$+\mu m_B(p_{n3}\ddot{p}_{n2}-p_{n2}\ddot{p}_{n3})$$
$$+T_{n1}-\mu p_{n2}F_{n3}+\mu p_{n3}F_{n2} \qquad (33)$$

$$(N_{12}-\mu m_B p_{n1}p_{n2})\dot{\omega}_{INn1}$$
$$+\left[N_{22}+\mu m_B\left(p^{\,2}_{n1}+p^{\,2}_{n3}\right)\right]\dot{\omega}_{INn2}$$
$$+N_{23}-\mu m_B p_{n2}p_{n3})\dot{\omega}_{INn3}=$$
$$(N_{23}-\mu m_B p_{n2}p_{n3})\omega_{INn1}\omega_{INn2}+$$
$$\left[N_{33}-N_{11}+\mu m_B\left(p^{\,2}_{n1}-p^{\,2}_{n3}\right)\right]\omega_{INn1}\omega_{INn3}$$
$$-(N_{12}-\mu m_B p_{n1}p_{n2})\omega_{INn2}\omega_{INn3}$$
$$+(N_{13}-\mu m_B p_{n1}p_{n3})(\omega^2_{INn1}-\omega^2_{INn3})$$
$$-N_{12}\ddot{\phi}+\dot{\phi}[2(N_{13}\omega_{INn1}+N_{23}\omega_{INn2})+$$
$$(N_{33}-N_{22}-N_{11})\omega_{INn3}]+N_{13}\dot{\phi}^2$$
$$+2\mu m_B\dot{p}_{n2}(\omega_{INn1}p_{n1}+\omega_{INn3}p_{n3})$$
$$-2\mu m_B\omega_{INn2}(p_{n1}\dot{p}_{n1}+p_{n3}\dot{p}_{n3})$$
$$-\mu m_B(p_{n3}\ddot{p}_{n1}-p_{n1}\ddot{p}_{n3})+T_{n2}$$
$$-\mu p_{n3}F_{n1}+\mu p_{n1}F_{n3} \qquad (34)$$

$$(N_{13}-\mu m_B p_{n1}p_{n3})\dot{\omega}_{INn1}+$$
$$(N_{23}-\mu m_B p_{n2}p_{n3})\dot{\omega}_{INn2}+$$
$$\left[N_{33}+\mu m_B\left(p^{\,2}_{n1}+p^{\,2}_{n2}\right)\right]\dot{\omega}_{INn3}=$$
$$\left[N_{11}-N_{22}+\mu m_B\left(p^{\,2}_{n2}-p^{\,2}_{n1}\right)\right]\omega_{INn1}\omega_{INn2}$$
$$-(N_{23}-\mu m_B p_{n2}p_{n3})\omega_{INn1}\omega_{INn3}$$
$$+(N_{13}-\mu m_B p_{n1}p_{n3})\omega_{INn2}\omega_{INn3}$$
$$+(N_{12}-\mu m_B p_{n1}p_{n2})(\omega^2_{INn2}-\omega^2_{INn1})$$

$$-N_{13}\ddot{\phi}-\dot{\phi}\left[2\left(N_{12}\omega_{INn1}+N_{23}\omega_{INn3}\right)+\left(N_{33}+N_{11}-N_{22}\right)\omega_{INn2}\right]-N_{12}\dot{\phi}^2$$
$$+2\mu m_B\dot{p}_{n3}\left(\omega_{INn1}p_{n1}+\omega_{INn2}p_{n2}\right)$$
$$-2\mu m_B\omega_{INn3}\left(p_{n1}\dot{p}_{n1}+p_{n2}\dot{p}_{n2}\right)$$
$$+\mu m_B\left(p_{n2}\ddot{p}_{n1}-p_{n1}\ddot{p}_{n2}\right)+T_{n3}+$$
$$-\mu p_{n1}F_{n2}+\mu p_{n2}F_{n1} \qquad (35)$$

Definitions of entities different than those defined in the rolling frame equations follow.

The inertial angular velocity of N is

$$\overline{{}^{I}\omega}^{N}=\omega_{INn1}\bar{n}_1+\omega_{INn2}\bar{n}_2+\omega_{INn3}\bar{n}_3 \qquad (36)$$

The inertial velocity of B* is

$$\overline{{}^{I}v}^{B^*}=v_{n1}\bar{n}_1+v_{n2}\bar{n}_2+v_{n3}\bar{n}_3 \qquad (37)$$

The aerodynamic force is given by

$$\bar{F}_{aero}=F_{n1}\bar{n}_1+F_{n2}\bar{n}_2+F_{n3}\bar{n}_3 \qquad (38)$$

The moment from this force about B* is

$$\bar{T}_{B^*}=T_{n1}\bar{n}_1+T_{n2}\bar{n}_2+T_{n3}\bar{n}_3 \qquad (39)$$

The inertia dyadic of B for B* and for N frame unit vectors is given by

$$\bar{I}^{B/B^*}=N_{11}\bar{n}_1\bar{n}_1+N_{12}\left(\bar{n}_1\bar{n}_2+\bar{n}_2\bar{n}_1\right)+$$
$$N_{13}\left(\bar{n}_1\bar{n}_3+\bar{n}_3\bar{n}_1\right)+N_{22}\bar{n}_2\bar{n}_2+$$
$$N_{23}\left(\bar{n}_2\bar{n}_3+\bar{n}_3\bar{n}_2\right)+N_{33}\left(\bar{n}_3\bar{n}_3\right) \qquad (40)$$

where

$$N_{11}=B_{11} \qquad (41)$$
$$N_{12}=B_{12}\cos(\phi)-B_{13}\sin(\phi) \qquad (42)$$
$$N_{13}=B_{12}\sin(\phi)+B_{13}\cos(\phi) \qquad (43)$$
$$N_{22}=B_{22}\cos^2(\phi)+B_{33}\sin^2(\phi)$$
$$-2B_{23}\sin(\phi)\cos(\phi) \qquad (44)$$
$$N_{23}=\left(B_{22}-B_{33}\right)\sin(\phi)\cos(\phi)$$
$$+B_{23}[\cos^2(\phi)-\sin^2(\phi)] \qquad (45)$$
$$N_{33}=B_{22}\sin^2(\phi)+B_{33}\cos^2(\phi)$$
$$+2B_{23}\sin(\phi)\cos(\phi) \qquad (46)$$

Elements of the direction cosine matrix relating the N frame to the G frame appearing in equations 30 through 32 are

$$G_{X_{31}}^{N}=-\sin(\theta) \qquad (47)$$
$$G_{X_{32}}^{N}=0 \qquad (48)$$
$$G_{X_{33}}^{N}=\cos(\theta) \qquad (49)$$

Autopilot Equations

The autopilot equations are a set of mathematical relationships that relate the angles-of-attack and side-slip in the nonrolling frame to the mass motion in the body-fixed frame. In this manner, the guidance commands can be directly related to the actuator commands. The autopilot equations are obtained by linearizing the nonrolling equations of motion (Equations 30 through 35) that were derived in the preceding section. The result of the linearizing procedure is a set of linear, time-varying equations that describe nonrolling angles-of-attack and side-slip of the ballistic vehicle.

The linearization procedure follows Reference 7 and begins with several simplifying assumptions:

1. The effects of gravity are negligible
2. The vehicle experiences only small angular perturbations ($\alpha, \beta << 1$ radian and ω_{INn2}, ω_{INn3}, v_{n2}, and v_{n3} are small perturbation quantities)
3. The moment of inertia tensor is symmetric with $I = N_{22} = N_{33}$ and $I_{xx} = N_{11}$
4. The mass only moves radially (p_{n1} = constant and $\dot{p}_{n1} = \ddot{p}_{n1} = 0$) and $m_p/m_s << 1$
5. The nonrolling roll rate is constant ($\dot{\omega}_{INn1} = 0$) and equal to zero, and $\ddot{\phi}$ is small (this will be justified later)
6. The vehicle has linear aerodynamics and retains basic aerodynamic symmetry with respect to the longitudinal axis, which implies that aerodynamic asymmetries are small ($\left|C_{m_o}/C_{m_\alpha}\right|, \left|C_{n_o}/C_{m_\alpha}\right| << 1$).

Using the first two and the fifth assumptions and neglecting nonlinear terms, the translational equations of motion become

$$F_{n1} = m_s v_{n1} \tag{50}$$

$$F_{n2} = m_s (\dot{v}_{n2} + \omega_{INn3} v_{n1}) + m_B \dot{\phi} \dot{p}_{n3} \tag{51}$$

$$F_{n3} = m_s (\dot{v}_{n3} - \omega_{INn2} v_{n1}) - m_B \dot{\phi} \dot{p}_{n2}. \tag{52}$$

The third through the fifth assumptions lead to the following transverse rate equations.

$$M'_{n2} = I' \dot{\omega}_{INn2} + I_{xx} \dot{\phi} \omega_{INn3} - \mu m_B p_{n1} \ddot{p}_{n3} \tag{53}$$

$$M'_{n3} = I' \dot{\omega}_{INn3} - I_{xx} \dot{\phi} \omega_{INn2} + \mu m_B p_{n1} \ddot{p}_{n2} \tag{54}$$

where

$$M'_{n2} = T_{n2} + \mu p_{n1} F_{n3} - \mu p_{n3} F_{n1}$$

$$M'_{n3} = T_{n3} - \mu p_{n1} F_{n2} + \mu p_{n2} F_{n1}$$

$$I' = I + \mu m_B p_{n1}^2$$

$$\mu = m_P / m_s$$

At this point, the nonrolling angles-of-attack and side-slip are defined as

$$\alpha = \tan^{-1} (v_{n3} / v_{n1}), \text{ and}$$

$$\beta = \sin^{-1} (v_{n2} / V)$$

where

$$V = \left[v_{n1}^2 + v_{n2}^2 + v_{n3}^2 \right]^{1/2}.$$

The relationships are linearized by applying assumption 2,

$$V \cong v_{n1}, \tag{55}$$

$$\alpha \cong v_{n3} / V, \text{ and} \tag{56}$$

$$\beta \cong v_{n2} / V. \tag{57}$$

Next, equations 55, 56, and 57 are differentiated to produce

$$\dot{V} \cong F_{n1} / m_s \tag{58}$$

$$\dot{\alpha} \cong \dot{v}_{n3} / V - \alpha F_{n1} / m_s V \tag{59}$$

$$\dot{\beta} \cong \dot{v}_{n2} / V - \beta F_{n1} / m_s V, \tag{60}$$

and complex notation is used to produce a more compact formulation for the angles-of-attack and side-slip, and the body rates

$$\bar{\zeta} = \beta + i\alpha = \frac{v_{n2} + i v_{n3}}{V}, \tag{61}$$

$$\frac{\dot{v}_{n2} + i\dot{v}_{n3}}{V} = \dot{\beta} + i\dot{\alpha} + \frac{F_{n1}}{m_s V} (\beta + i\alpha), \text{ and} \tag{62}$$

$$\bar{\Omega} = \omega_{INn2} + i\omega_{INn3} \tag{63}$$

Equations 51 through 54 are written in complex notation as

$$F_{n2} + iF_{n3} = m_s \left[(\dot{v}_{n2} + i\dot{v}_{n3}) - i v_{n1} (\omega_{INn2} + i\omega_{INn3}) \right] + m_B \dot{\phi} (\dot{p}_{n3} - i\dot{p}_{n2})$$

$$M'_{n2} + iM'_{n3} = I' (\dot{\omega}_{INn2} + i\dot{\omega}_{INn3}) - iI_{xx} \dot{\phi} (\omega_{INn2} + i\omega_{INn3}) - \mu m_B p_{n1} (\ddot{p}_{n3} - i\ddot{p}_{n2})$$

Upon substitution of equations 61 through 63, one obtains

$$\frac{F_{n2} + iF_{n3}}{m_s V} = \dot{\bar{\zeta}} + \frac{F_{n1}}{m_s V} \bar{\zeta} - i\bar{\Omega} + K_3 (\ddot{p}_{n3} - i\ddot{p}_{n2}) \tag{64}$$

$$\frac{M'_{n2}+iM'_{n3}}{I'} = \dot{\bar{\Omega}} - iK_1\bar{\Omega} - K_2(\dot{p}_{n3} - i\dot{p}_{n2}) \tag{65}$$

where

$$K_1 = \frac{I_{xx}}{I'}\dot{\phi},$$

$$K_2 = \frac{\mu m_B}{I'}p_{n1}, \text{ and } K_3 = \frac{m_B\dot{\phi}}{m_s V}$$

The next step is to specify the form of the aerodynamic forces and moments of equations 64 and 65 in terms of $\bar{\zeta}, \bar{\Omega}$, and their time derivatives. By applying assumption 6, the aerodynamic forces and moments are defined as

$$F_{n1} = -qSC_A$$

$$F_{n2} = qS(C_{y_o} + C_{y_\beta}\beta)$$

$$F_{n3} = qS(C_{z_o} + C_{z_\alpha}\alpha)$$

$$T_{n2} = qSd\left[C_{m_0} + C_{m_\alpha}\alpha + C_{m_{\dot{\alpha}}}\left(\frac{\dot{\alpha}d}{2V}\right)\right.$$

$$\left. + C_{m_{\alpha_{INn2}}}\left(\frac{\omega_{INn2}d}{2V}\right) + C_{m_{\dot{\phi}\beta}}\beta\left(\frac{\dot{\phi}d}{2V}\right)\right]$$

$$T_{n3} = qSd\left[C_{n_o} + C_{n_\beta}\beta + C_{n_{\dot{\beta}}}\left(\frac{\dot{\beta}d}{2V}\right)\right.$$

$$\left. + C_{n_{\alpha_{INn3}}}\left(\frac{\omega_{INn3}d}{2V}\right) + C_{n_{\dot{\phi}\alpha}}\alpha\left(\frac{\dot{\phi}d}{2V}\right)\right]$$

where

$$q = \frac{1}{2}\rho V^2$$

ρ = atmospheric density

S = cross sectional area

d = reference length,

and the zero-subscripted terms account for small aerodynamic asymmetries. These aerodynamic forces and moments can be simplified by applying the aerodynamic symmetry assumption to obtain

$$C_{y_\beta} = C_{z_\alpha} = -C_{N_\alpha},$$

$$C_{n_\beta} = -C_{m_\alpha},$$

$$C_{n_{\dot{\beta}}} = -C_{m_{\dot{\alpha}}},$$

$$C_{n_{\omega_{INn3}}} = C_{m_{\omega_{INn3}}}, \text{ and}$$

$$C_{n_{\dot{\phi}\alpha}} = C_{m_{\dot{\phi}\beta}}$$

The left sides of equations 64 and 65 can now be evaluated by substituting the definitions given above.

$$F_{n2} + iF_{n3} = qS\left[C_{y_o} + iC_{z_o} - C_{N_\alpha}\bar{\zeta}\right] \tag{66}$$

$$M'_{n2} + iM'_{n3} = qS\left[d\,(C_{m_o} + iC_{n_o})\right.$$

$$+ \mu p_{n1}(C_{z_o} - iC_{y_o}) + \mu C_A\,(p_{n3} - ip_{n2})$$

$$+ i(\mu p_{n1}C_{N_\alpha} - C_{m_\alpha}d)\bar{\zeta}$$

$$+ C_{m_{\omega_{INn2}}}\left(\frac{d^2}{2V}\right)\dot{\bar{\Omega}} - iC_{m_{\dot{\alpha}}}\left(\frac{d^2}{2V}\right)\dot{\bar{\zeta}}$$

$$\left. + C_{m_{\dot{\phi}\beta}}\left(\frac{\dot{\phi}d^2}{2V}\right)\bar{\zeta}\right] \tag{67}$$

Equations 64 and 66 can be algebraically manipulated to give a relationship between $\bar{\Omega}$ and $\bar{\zeta}$.

$$\bar{\Omega} = -i\dot{\bar{\zeta}} + i\left(\frac{qS}{m_s V}\right)\left[C_A - C_{N_\alpha}\right]\bar{\zeta} +$$

$$i\left(\frac{qS}{m_s V}\right)[C_{y_o} + iC_{z_o}] - K_3(\dot{p}_{n2} + i\dot{p}_{n3}) \tag{68}$$

The substitution of equation 68 and its first derivative, along with equation 67 into equation 65, produces the desired linear, time-varying autopilot equation

$$\ddot{\bar{\zeta}} + \bar{A}\dot{\bar{\zeta}} + \bar{B}\bar{\zeta} = \bar{C} \tag{69}$$

where

$$\bar{A} = -\left[\frac{qS}{m_s V}(C_A - C_{N_\alpha}) + \frac{qSd^2}{2VI'}\left(C_{m_q} + C_{m_{\omega_{INn2}}}\right) + iK_1\right]$$

$$\bar{B} = -\left[\frac{qS}{m_s V}(C_A - C_{N_\alpha}) + \left(\frac{qSC_A}{m_s V}\right)^2\left(1 - \frac{C_{N_\alpha}}{C_A}\right) - \left(\frac{qSd}{V}\right)^2\left(\frac{C_{m_{\omega_{INn2}}}}{2m_s I'}\right)(C_A - C_{N_\alpha}) + \frac{qS}{I'}(C_{m_\alpha} d - C_{N_\alpha}\mu p_{n1}) + i\left(\frac{-qSK_1}{m_s V}(C_A - C_{N_\alpha}) + \frac{qSd^2}{2VI'}\dot{\phi}C_{m_{\dot{\phi}\beta}}\right)\right]$$

$$\bar{C} = (C_{y_0} + iC_{z_0})\left[\left(\frac{qS}{m_s V}\right) + \left(\frac{qS}{m_s V}\right)^2 C_A - \left(\frac{qSd}{V}\right)^2\left(\frac{C_{m_{\omega_{INn2}}}}{2m_s I'}\right) - i\frac{qS}{m_s V}K_1\right] - \frac{qSd}{I'}(C_{n_\alpha} - i\bar{C}_{m_\alpha}) + \frac{qS}{I'}\mu p_{n1}(C_{y_\alpha} + iC_{z_\alpha}) + \frac{qS}{I'}\mu C_A(p_{n2} + ip_{n3}) + \left[K_1K_3 + i\dot{K}_3\right](\dot{p}_{n2} + i\dot{p}_{n3}) + [K_2 + iK_3](\ddot{p}_{n2} + i\ddot{p}_{n3}),$$

and the nonrolling mass position is defined in terms of the body-fixed mass position as

$$\underline{p}^N = \begin{pmatrix} 0 \\ p_{b2}c\phi - p_{b3}s\phi \\ p_{b2}s\phi + p_{b3}c\phi \end{pmatrix} \quad (70)$$

$$\underline{\dot{p}}^N = \begin{pmatrix} 0 \\ (\dot{p}_{b2} - p_{b3}\dot{\phi})c\phi - (\dot{p}_{b3} + p_{b2}\dot{\phi})s\phi \\ (\dot{p}_{b2} - p_{b3}\dot{\phi})s\phi + (\dot{p}_{b3} + p_{b2}\dot{\phi})c\phi \end{pmatrix} \quad (71)$$

$$\underline{\ddot{p}}^N = \begin{pmatrix} 0 \\ (\ddot{p}_{b2} - p_{b2}\dot{\phi}^2 - 2\dot{p}_{b3}\dot{\phi} - p_{b3}\ddot{\phi})c\phi - (2\dot{p}_{b2}\dot{\phi} + p_{b2}\ddot{\phi} + \dot{p}_{b3} - p_{b3}\dot{\phi}^2)s\phi \\ (\ddot{p}_{b2} - p_{b2}\dot{\phi}^2 - 2\dot{p}_{b3}\dot{\phi} - p_{b3}\ddot{\phi})s\phi + (2\dot{p}_{b2}\dot{\phi} + p_{b2}\ddot{\phi} + \dot{p}_{b3} - p_{b3}\dot{\phi}^2)c\phi \end{pmatrix} \quad (72)$$

where $c\phi = \cos(\phi)$ and $s\phi = \sin(\phi)$.

The last step is to justify the assumption that $\ddot{\phi}$ is small. By linearizing the nonrolling roll rate equation, the following relationship is derived,

$$I_{xx}\ddot{\phi} = T_{n1} + \mu\left[p_{n3}F_{n2} - p_{n2}F_{n3}\right]$$

$$\ddot{\phi} = \frac{qS}{I_{xx}}\left[C_{l_o}d + C_{l_{\dot{\phi}}}\left(\frac{\dot{\phi}d^2}{2V}\right) + \mu(C_{y_o}p_{n3} - C_{z_o}p_{n2})\right] \quad (73)$$

which demonstrates that $\ddot{\phi}$ is small for small aerodynamic asymmetries and roll torques.

Evaluation of Autopilot Equations

The goal of this section is to derive a set of theoretical design tools for choosing and sizing MMTC systems. The first step is to solve equation 69 for the steady-state complex AOA. If one considers a slender vehicle ($I' >> I_{xx}$) that flies along a constant flight path angle through an exponential atmosphere, then the $\bar{B}$ term reduces to

$$\bar{B} = -qS\left[\frac{1}{I'}(C_{m_\alpha}d - C_{N_\alpha}\mu p_{n1}) +\right.$$

$$i\left\{\frac{K_1}{m_s V}(C_A - C_{N_\alpha}) + \frac{d^2}{2VI'}\dot{\phi}C_{m_{\dot{\phi}\beta}}\right\}\Bigg]$$

and neglecting aerodynamic asymmetries, the $\bar{C}$ term becomes

$$\bar{C} = \bar{C}_1 + \bar{C}_2 \text{ where}$$

$$\bar{C}_1 = \frac{qS}{I'}\mu C_A (p_{n2} + ip_{n3}) \text{ and}$$

$$\bar{C}_2 = [K_1 K_3 + i\dot{K}_3](\dot{p}_{n2} + i\dot{p}_{n3}) + [K_2 + iK_3](\ddot{p}_{n2} + i\ddot{p}_{n3})$$

The steady-state complex AOA is

$$\bar{\zeta}_T = \frac{\bar{C}}{\bar{B}} \tag{74}$$

where

$$\bar{\zeta}_T = \bar{\zeta}_{T_1} + \bar{\zeta}_{T_2} = \frac{\bar{C}_1}{\bar{B}} + \frac{\bar{C}_2}{\bar{B}}$$

where $\bar{\zeta}_{T_1}$ is the trim angle contribution due to center of mass offset and ζ_{T_2} is the contribution due to PAM. The major contribution of $\bar{\zeta}_{T_1}$ to $\bar{\zeta}_T$ is defined by setting the body-fixed roll rate to zero $(\dot{\phi} = 0)$ and assuming the mass is not moving in the body-fixed frame to obtain

$$\bar{\zeta}_{T_1} = \frac{-\mu C_A (p_{n2} + ip_{n3})}{(C_{m_\alpha} d - C_{N_\alpha}\mu p_{n1})}$$

or

$$\alpha_{T_1} = \frac{-\mu C_A p_{n3}}{(C_{m_\alpha} d - C_{N_\alpha}\mu p_{n1})} \tag{75}$$

$$\beta_{T_1} = \frac{-\mu C_A p_{n2}}{(C_{m_\alpha} d - C_{N_\alpha}\mu p_{n1})} \tag{76}$$

The major contribution of $\bar{\zeta}_{T_2}$ to $\bar{\zeta}_T$ is difficult to evaluate in the nonrolling frame, but can be determined in the body-fixed frame. The limiting trim angle is given by Hodapp [7] and is equal to the PAM angle.

$$\left|\zeta_{T_2}\right| \cong \frac{m_p p_{n1}}{I'} p_{n23} \tag{77}$$

where p_{n23} is the largest radial displacement of the moving mass.

As a result, one can expect to obtain an AOA that is approximately equal to the PAM angle if the moving mass can be manipulated properly. The proper manipulation of the mass will be described in the next section.

The theoretical design tools, or rules-of-thumb, are equations 75 through 77. Equations 75 and 76 are used to size an MMTC for slow spinning ballistic vehicles that have small static margins (SM < 10% of body length), while equation 77 is employed for fast spinning vehicles that have static margins greater than 10% of body length. The dividing line between slow and fast spinning is the critical roll rate:

$$\omega_{cr} = \left[\frac{-C_{m_\alpha} qSd}{I' - I_{xx}}\right]^{1/2} \tag{78}$$

This dividing line determines the dominance of either aerodynamic or inertial forces and moments. The aerodynamic forces dominate when the body-fixed roll rate is below ω_{cr}, whereas the inertial forces dominate when the roll rate is above ω_{cr}. Consequently, one is designing an MMTC that is either a trim due to drag system (subcritical) or a trim due to PAM system (supercritical).

Performance Examples

The first step in sizing an MMTC is to perform 3DOF trajectory simulations of the ballistic vehicle to determine the required trim AOA for a given divert capability. The results of 3DOF simulations for a sphere-cone RV and a rocket are presented in Figures 2 through 5. The divert capability for an RV is strongly influenced by the flight path angle and the divert initiation altitude. The steeper trajectories require more AOA for the same divert capability, and there is an upper divert initiation altitude limit at approximately 90 kft. The results of the rocket simulations show an interesting correlation between pre- and post-apogee maneuvers and down-

range and crossrange divert capability. The pre-apogee maneuvers generate mostly downrange dispersion while post-apogee maneuvers produce mostly crossrange dispersion. Given these relationships between divert capability and AOA, one can employ the rules-of-thumb of the previous section to design MMTCs for ballistic vehicles.

Subcritical Control (RV)

As stated earlier, the subcritical control example is a sphere-cone RV. Equation 75 is used to calculate the approximate relationship between the steady-state trim AOA and the required mass moment. The results are displayed in Figure 6. The required mass moment is a linear function of the AOA, and the slope of the line becomes steeper as the SM is decreased. For this example, the desired divert capability is 1150 ft which corresponds to a trim AOA of 0.22° for a flight path angle of -41°, a mass moment of 170 lbm-in, and a static margin of 8%. The MMTC was designed with a maximum radial stroke of 7 in. and a 24-lbm moving mass. The simulation results of the RV MMTC with a simple autopilot that holds the moving mass fixed in the nonrolling frame in the crossrange direction are presented in Figures 7 through 11. Figure 7 confirms that the MMTC delivers the desired crossrange divert while Figure 8 shows minimal downrange change. Figure 9 verifies the desired trim AOA performance. Figures 10 and 11 show that the divert initiation altitude was 50 kft and the roll rate performance is stable.

Three conceptual layouts for the RV MMTC are presented in Figure 12. The first and third layouts require two moving masses while the second uses a single mass. The approximate layout for a given RV depends on the application.

Supercritical Control (Rocket)

The supercritical performance example is a fast spinning rocket. Equation 77 is used to calculate the approximate relationship between the trim AOA and the required PAM. The results for a sea level flight are presented in Figure 13. Since the rocket is flying through a varying atmosphere (from 0 to 40,000 ft), the sizing of the mass must be iterated upon using the simulation. For this example, the desired divert capability is 8000 ft which corresponds to a trim AOA of 0.35° for control after burnout to impact. This required trim AOA is an average value over the trajectory, and the peak AOA is approximately an order of magnitude larger than the value given by equation 77. The MMTC was designed with a maximum stroke of 4 in. and a 5-lbm moving mass which produces a cross product of inertia equal to 1200 lb-in^2. The simulation results of the rocket MMTC are displayed in Figures 14 through 17. Figure 14 confirms that the PAM MMTC provides the desired crossrange divert while the trim due to drag MMTC produces nearly zero divert. Figure 15 shows the AOA and side-slip angle performance match the prediction of equation 77 at low altitudes near launch and impact (AOA $\cong$ 0.1°) and follow the dynamic pressure profile (Figure 16) and the altitude history (Figure 17). The autopilot system in this MMTC simulation is more complicated than the RV MMTC since one is attempting to create inertial forces due to PAM in a nonrolling frame. This is a problem because the inertial forces rely on the roll rate squared, and the nonrolling roll rate is approximately zero. The way to overcome this problem is to articulate the mass in the body-fixed frame such that the mass is held fixed over a portion of the cycle in the desired direction. The motion of the mass is presented in Figure 18. This cyclic motion accounts for the cyclic variation of the AOA. This autopilot can be characterized as a "bang-bang" type of control system where the AOA is controlled by the number of times the mass is actuated in a given direction. The conceptual layout is a relatively simple one as most bang-bang actuators are in practical applications. Figure 19 shows a single mass that slides in a piston tube behind the warhead section.

Summary

The focus of this work was to assess the feasibility of MMTCs to increase the accuracy of axisymmetric, ballistic vehicles. A general set of equations of motion for a single moving mass was derived in the body-fixed and nonrolling frames. These equations of motion were linearized and manipulated to produce a general set of autopilot equations that relate the motion of the moving mass in the body-fixed frame to the AOA and side-slip angle in the nonrolling frame. These autopilot equations can be used to develop closed-loop control systems for the MMTCs.

The assessment began by evaluating the effectiveness of aerodynamic versus inertial forces for different vehicles. A set of rules-of-thumb were developed that categorize the ballistic vehicles of interest. Basically, fast spinning vehicles use trim due to PAM because the body-fixed roll rate is above the critical roll rate and the inertial forces are dominant. The slow spinning vehicles employ trim due to drag since the roll rate is subcritical and the aerodynamic forces are dominant. One important point

about slow spinners is the SM must be sufficiently small (less than 10%) to produce a reasonably sized MMTC.

These design rules-of-thumb were verified by simulating MMTCs for a sphere-cone RV and a rocket. The RV MMTC performed as predicted by the design rules while the rocket MMTC predictions were low because the design rules assumed a constant atmosphere and a constant flight path angle. However, during each interval that these assumptions were valid, the predictions were accurate.

Finally, conceptual designs were presented that demonstrated the feasibility of MMTCs, given reasonable physical constraints. The MMTCs fit within the allowable volume and weighed only a few percent of the vehicle's total weight for these examples. Although these example cases demonstrated the feasibility of MMTCs, the most important aspect of this paper is the presentation of general design and analysis tools to evaluate prospective ballistic vehicles and MMTCs.

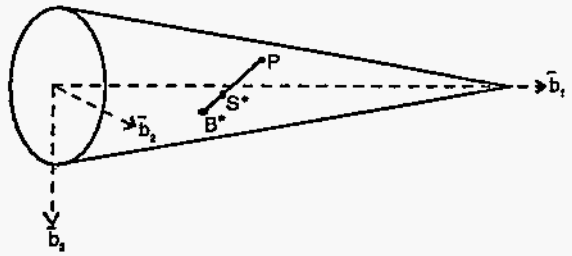

Fig. 1 Ballistic vehicle with one moving point mass

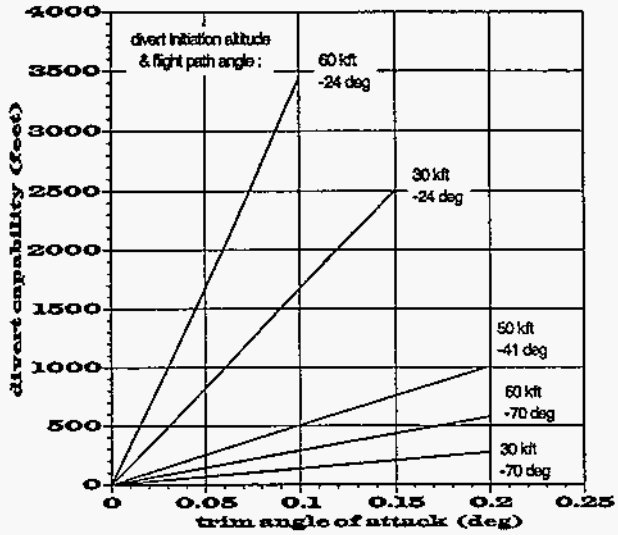

Fig. 2 RV: divert capability from various initial conditions

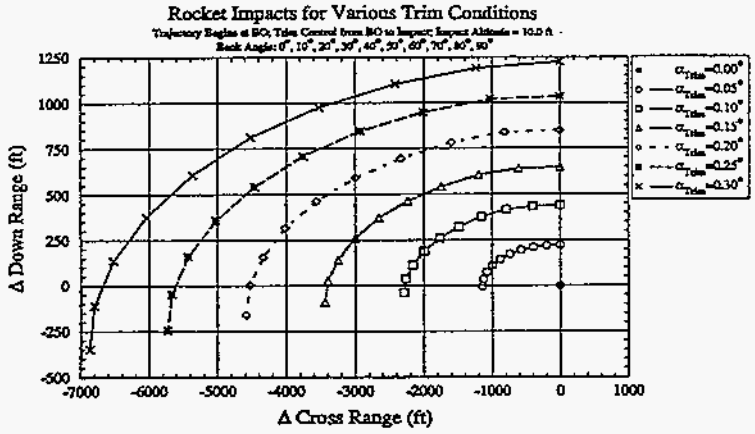

Fig. 3 Rocket with constant aerodynamic trim
(trim control from burnout to impact)

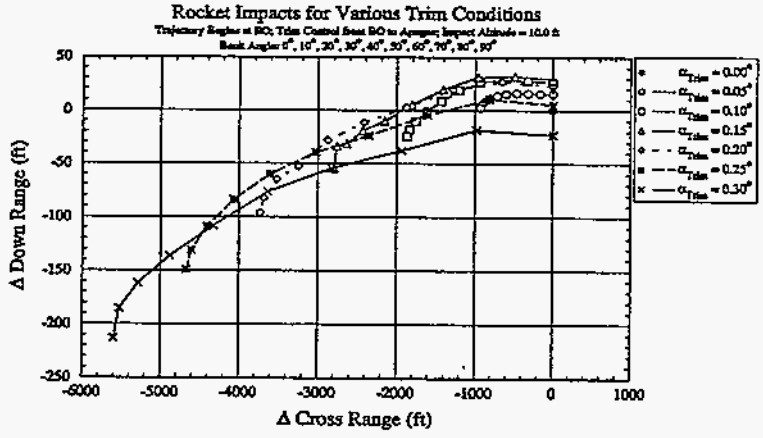

Fig. 4 Rocket with constant aerodynamic trim
(trim control from burnout to apogee)

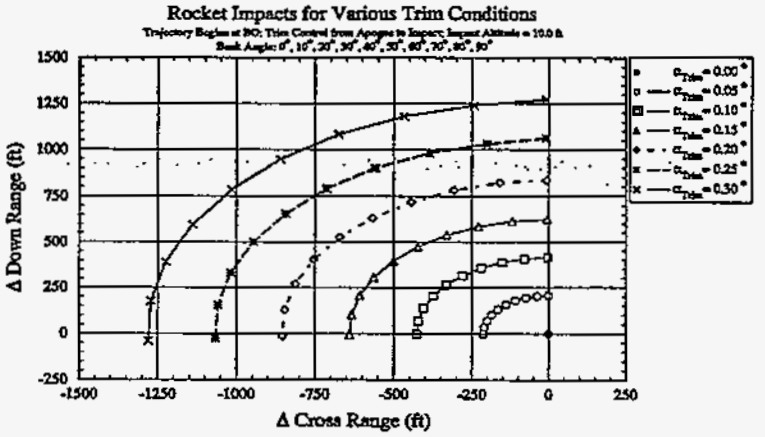

Fig. 5 Rocket with constant aerodynamic trim
(trim control from apogee to impact)

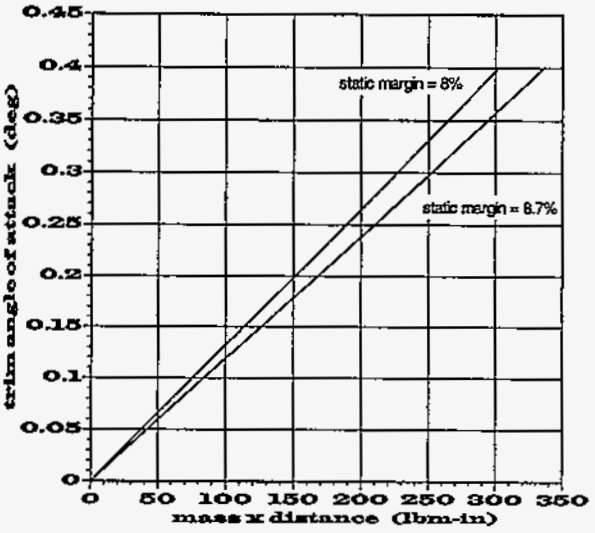

Fig. 6 RV: static trim capability

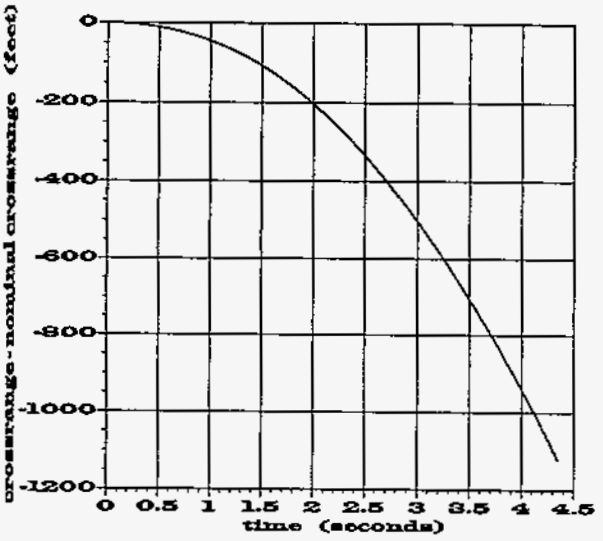

Fig. 7 RV: 24 lbm point mass offset 7 inches

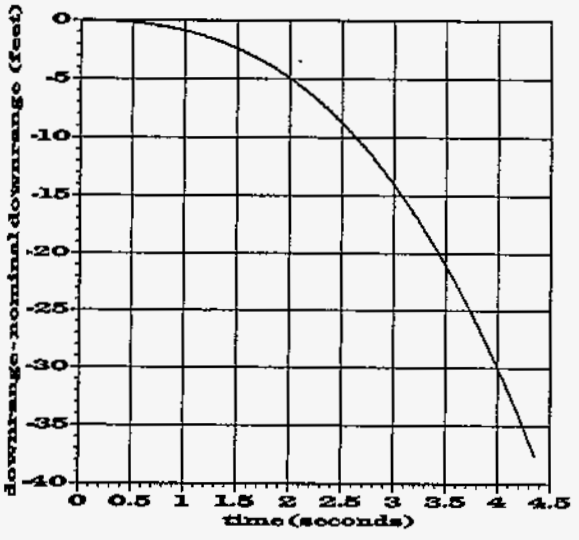

Fig. 8 RV: 24 lbm point mass offset 7 inches

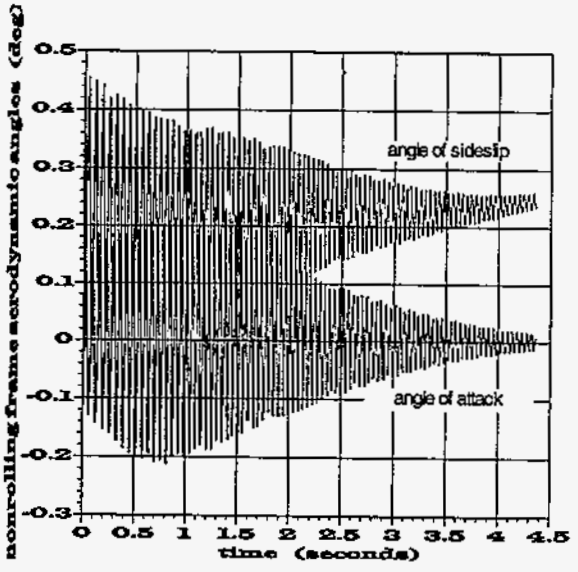

Fig. 9 RV: 24 lbm point mass offset 7 inches

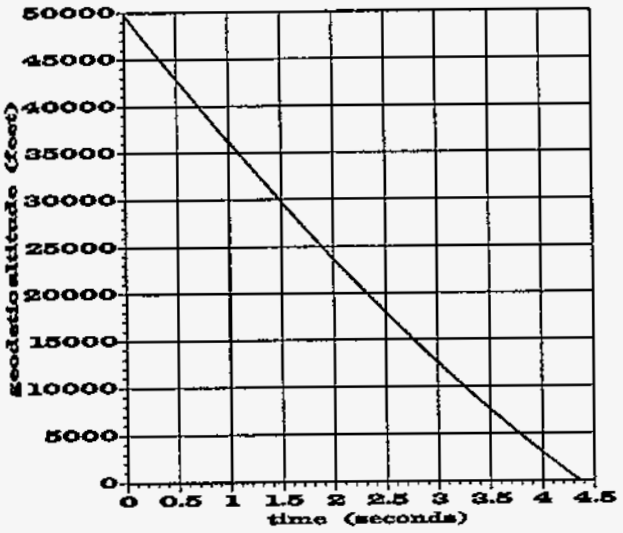

Fig. 10 RV: 24 lbm point mass offset 7 inches

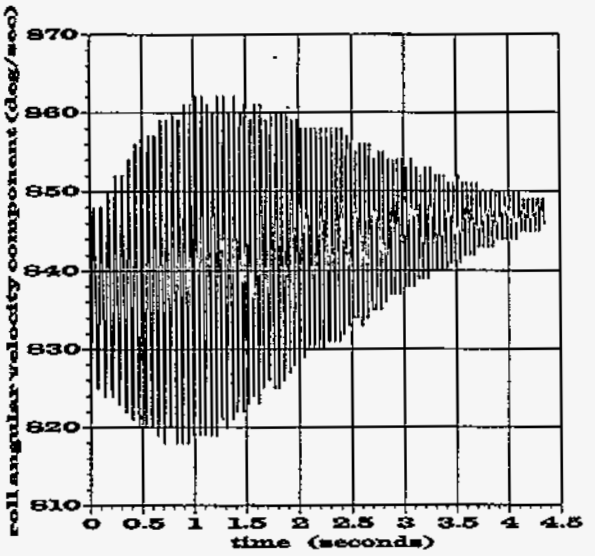

Fig. 11 RV: 24 lbm point mass offset 7 inches

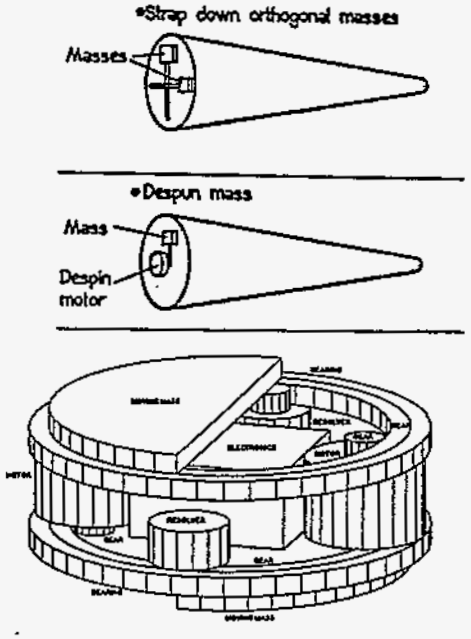

Fig. 12 Three moving mass layouts

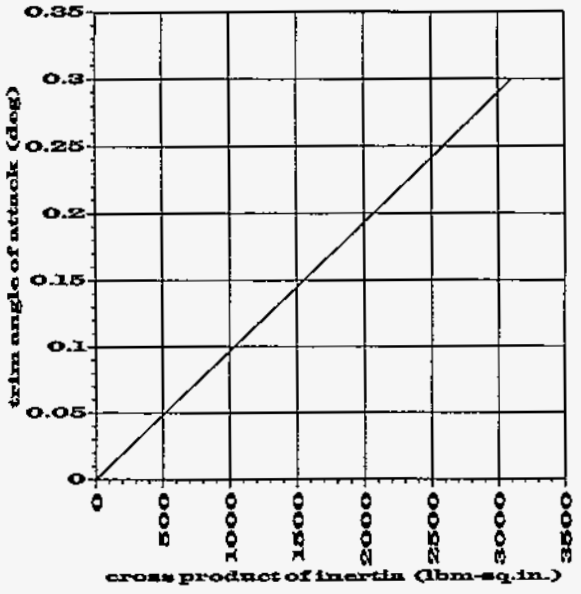

Fig. 13 rocket : effect of PAM on trim angle of attack

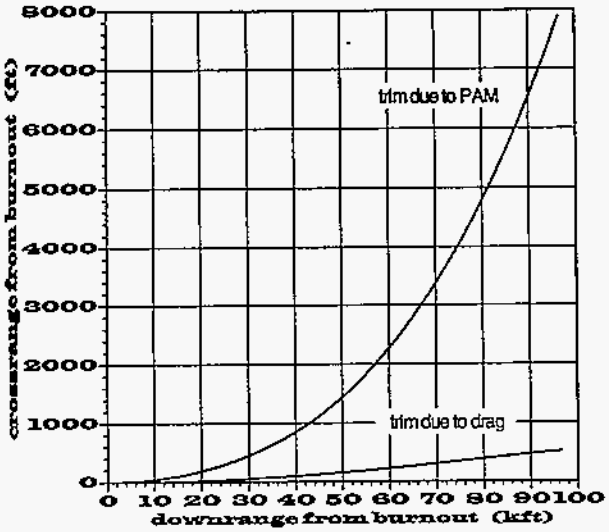

Fig. 14 rocket: 5 lbm point mass with 4 inch maximum offset

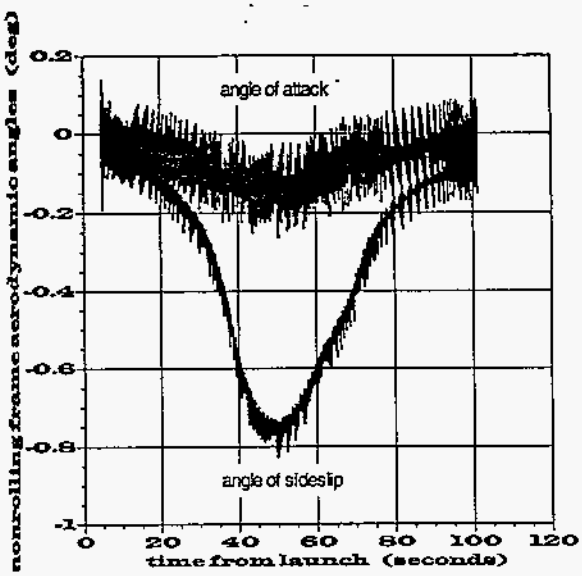

Fig. 15 rocket: 5 lbm point mass with 4 inch maximum offset

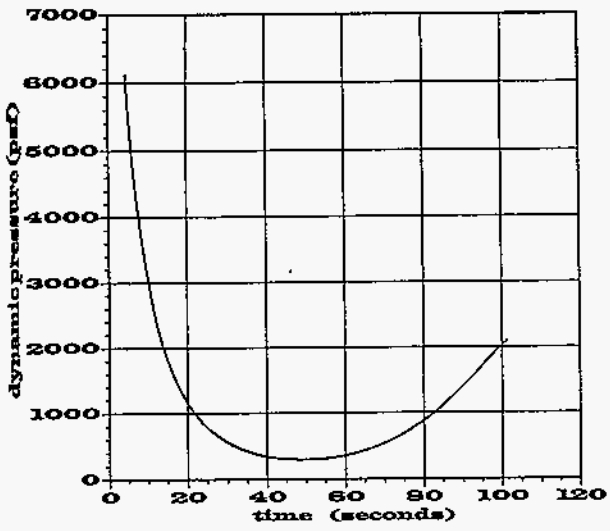

Fig. 16 rocket: 5 lbm point mass with 4 inch maximum offset

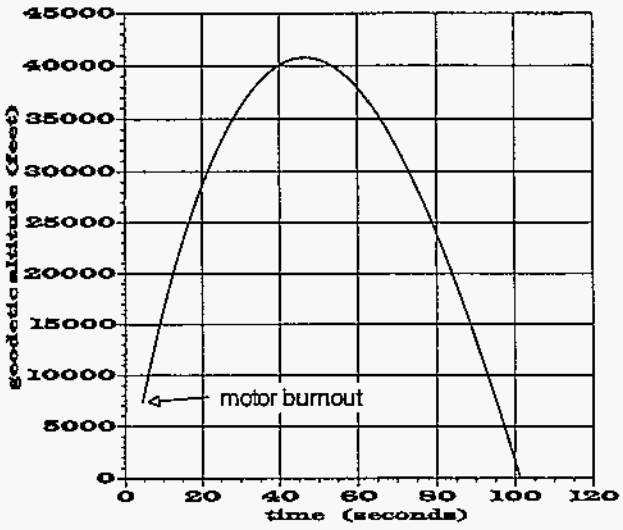

Fig. 17 rocket: 5 lbm point mass with 4 inch maximum offset

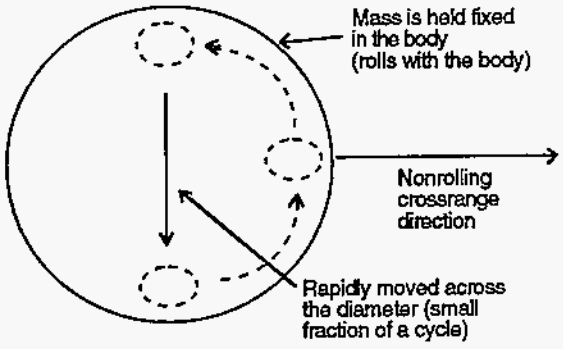

Fig. 18 Moving mass articulation

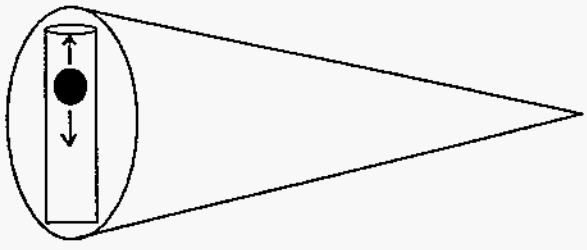

Fig. 19 Bang-bang actuator

References

1. F. J. Regan, *Re-entry Vehicle Dynamics*, AIAA Education Series, American Institute of Aeronautics and Astronautics, 1984.
2. R. D. Tucker, and A. F. Veneruso, *Analysis of a Proposed Movable Mass Reentry Vehicle Roll Control System*, Sandia National Laboratories Report, SC-RR-710090, March 1971.
3. T. Petsopoulos, and F. J. Regan, *A Moving-Mass Roll Control System for a Fxed-Trim Re-entry Vehicle*, AIAA-94-0033, 32nd Aerospace Sciences Meeting and Exhibit, January 1994.
4. F. J. Regan, *Private Communications*, July 1994.
5. J. E. White, and R. D. Robinett, III, *Principal Axis Misalignment Control for Deconing of Spinning Spacecraft*, Journal of Guidance, Control and Dynamics, Vol. 17, No. 4, July–August 1994.
6. Kane and Levinson, *Dynamics: Theory and Applications*, McGraw-Hill Book Company, 1985.
7. A. E. Hodapp, Jr. and E. L. Clark, Jr., *A Technique for Determining Approximate Roll Rate Histories for Ballistic Reentry Vehicles Having Mass, Inertia, and Aerodynamic Asymmetries*, Sandia National Laboratories Report, SC-RR-69-804, September 1970.